

# Dissection of Alkylpyridinium Structures to Understand Deamination Reactions

Sergei Tcyrlunikov, Qiuqi Cai, J. Cameron Twitty, Jianyu Xu, Abderrahman Atifi, Olivia P. Bercher, Glenn P. A. Yap, Joel Rosenthal,\* Mary P. Watson,\* and Marisa C. Kozlowski\*



Cite This: *ACS Catal.* 2021, 11, 8456–8466



Read Online

ACCESS |



Metrics & More



Article Recommendations

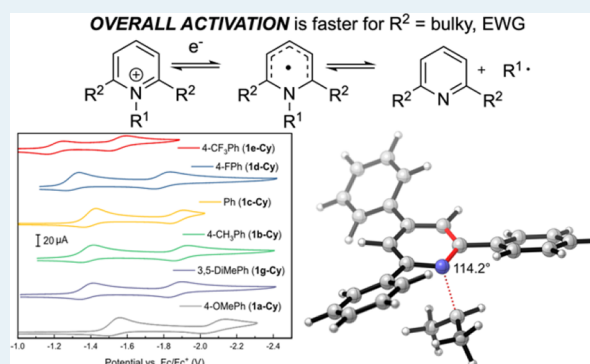


Supporting Information

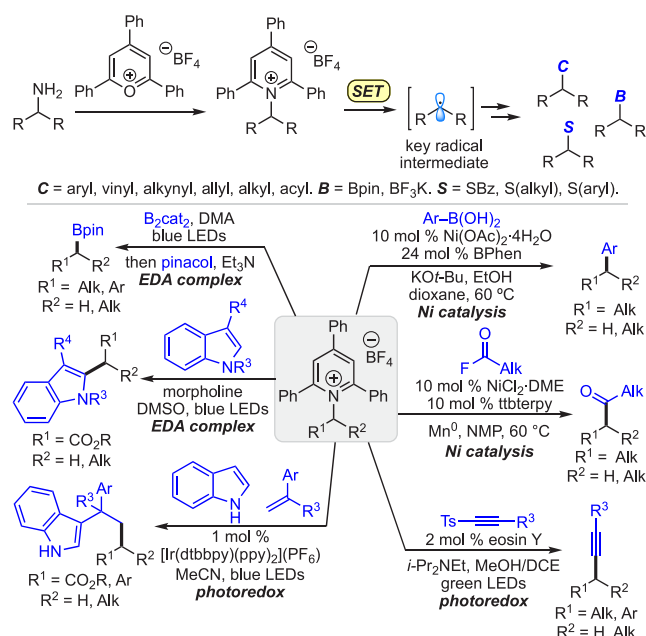
**ABSTRACT:** Via conversion to Katritzky pyridinium salts, alkyl amines can now be used as alkyl radical precursors for a range of deaminative functionalization reactions. The key step of all of these methods is single-electron reduction of the pyridinium ring, which triggers C–N bond cleavage. However, little has been done to understand how the precise nature of the pyridinium influences these events. Using a combination of synthesis, computation, and electrochemistry, this study delineates the steric and electronic effects that substituents have on the canonical steps and the overall process. Depending on the approach taken, consideration of both the reduction and the subsequent radical dissociation may be necessary. Whereas the electronic effects on these steps work in opposition to each other, the steric effects are synergistic, with larger substituents favoring both steps.

This understanding provides a framework for future design of pyridinium salts to match the mode of catalysis or activation.

**KEYWORDS:** deamination, pyridinium, single-electron transfer, electrochemical, radical fragmentation



## Scheme 1. Seminal Methods Using Alkylpyridinium Salts in Cross-Coupling



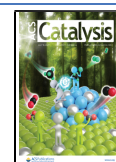
## INTRODUCTION

Amines have long been recognized as a useful substrate class for synthesis. In particular, the wide diversity of commercially available alkyl amines offers opportunities for the preparation of a variety of molecules in pharmaceutical discovery,<sup>1,2</sup> and the ubiquity of alkyl amines as advanced intermediates, biomolecules, and drugs provides opportunities for late-stage derivatization.<sup>3</sup> However, the use of alkyl amines has classically been limited to the synthesis of nitrogen-containing products. Until recently, deaminative methods were largely limited to alkyl amine derivatives with highly specific structural requirements surrounding the alkyl group or C–N bond (benzylic, allylic,  $\alpha$ -carbonyl, or strained).<sup>4</sup> However, the recognition that Katritzky pyridinium salts, or 2,4,6-triphenylpyridinium salts,<sup>5</sup> can be utilized as alkyl radical precursors has opened new opportunities in synthesis via deamination. Indeed, there has been a growing interest in Katritzky alkylpyridinium salts since our 2017 publication<sup>6</sup> demonstrating that they can be used in nickel-catalyzed cross-couplings.<sup>7</sup> Excitingly, the development

Received: April 23, 2021

Revised: June 8, 2021

Published: June 28, 2021



of these methods has demonstrated that the utility of pyridinium salts extends beyond serving as a pseudohalide; the pyridinium group can participate in activation modes unknown for halide counterparts. Methods to harness these largely untapped pyridinium reagents now utilize a variety of methods to activate the pyridinium ring via single-electron transfer (SET), including transition metal catalysis,<sup>8</sup> photoredox catalysis,<sup>9</sup> and photoactivation of electron donor–acceptor (EDA) pairs (Scheme 1).<sup>10</sup> Via these methods, amino groups can now be transformed to aryl, vinyl, alkynyl, allyl, alkyl, boryl, and carbonyl substituents.

However, limitations in this chemistry remain. The structure of the pyridinium moiety is largely dictated by the pyrylium precursors that are readily available, with 2,4,6-triphenylpyridinium salts nearly exclusively used. Although medicinal chemists have adopted these methods, the poor atom economy of the 2,4,6-triphenylpyridinium moiety hinders adoption in process chemistry and other large-scale synthesis. Further, the synthesis of 2,4,6-triphenylpyridinium salts is only possible for constrained tertiary alkyl groups with smaller steric footprints, such as cyclopropyls.<sup>8c,10b,11</sup> Finally, notable differences in reactivity between primary and secondary alkylpyridinium salts have been observed in certain activation classes. This trend is most prevalent under photoredox catalysis, where often only secondary alkylpyridinium salts undergo activation by the photocatalyst.<sup>8h,9a,b</sup> This trend is also found within transition metal catalysis, where different conditions are often needed to effect reactions with primary and secondary alkylpyridinium salts.<sup>8c,e–g</sup> These observations have precipitated some effort toward understanding the SET and C–N bond cleavage steps. To date, these studies have largely focused on the differences due to the alkyl substituent.<sup>5,12</sup> For example, in studying the requirement for secondary alkyl groups in their photoredox-catalyzed alkynylation, Gryko and co-workers observed complete reversibility in the electrochemical reduction of primary alkylpyridinium salts, while secondary alkyl and benzylic pyridinium salts exhibited quasireversible or irreversible cyclic voltammetry (CV) traces.<sup>9a</sup> This result is consistent with the increased difficulty associated with forming primary alkyl radicals.

In contrast, little effort has been directed toward understanding the role of the pyridinium ring itself on the reactivity of these compounds, with the recent use of tris(*p*-methoxyphenyl)pyridinium salt by Martin and co-workers as the sole exception.<sup>8g</sup> In his CV studies of these “tuned” pyridinium salts, the reduction of primary alkylpyridinium salts is again reversible, and that of secondary alkylpyridiniums is quasireversible. However, at elevated temperatures, the reversibility of this reduction decreased slightly, suggesting that temperature may play a role in the improved reactivity of the tris(4-methoxyphenyl) pyridinium salt. Despite this work, it remains unknown what implications further permutations of the pyridinium salt would have.

Given the tunability of the pyridinium moiety by means of different substituents and its importance in the activation process, a greater understanding of its role in controlling reactivity would be beneficial. Herein, we describe our detailed study of the effect of substitution on the pyridinium ring of secondary alkylpyridinium salts. We show that electronic effects play a crucial role in modulation of the reduction potential, while steric bulk at the 2,6-positions facilitates cleavage of the C–N bond. This work lays the foundation for fundamental understanding of the SET and C–N bond

cleavage steps to guide the development of future methods especially to enable the inclusion of problematic substrates.

## RESULTS AND DISCUSSION

In consideration of the structure and reactivity of alkylpyridiniums, several canonical steps are important. Specifically,

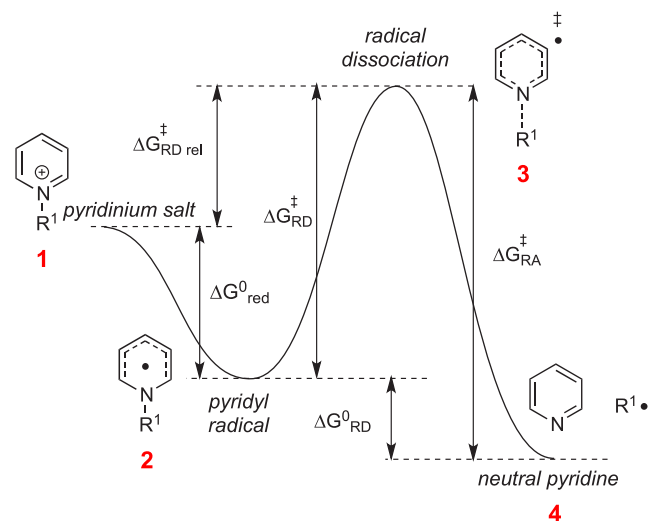
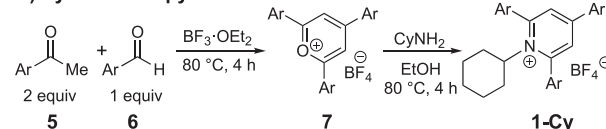


**Figure 1.** Generic energy profile for C–N bond activation and parameters discussed in this study.

## Scheme 2. Pyridinium Salts Used for Computational and Electrochemical Investigations

### A) Synthesis of pyridinium salts

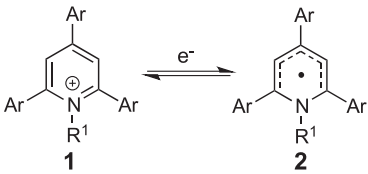


### B) Pyridinium salts used for computational and electrochemical investigations

Synthesized Compounds		Hypothetical Compounds	
Ar	Yield of 1-Cy <sup>a</sup>	R <sup>2</sup>	
1a 4-MeOC <sub>6</sub> H <sub>4</sub>	24%	1h <i>t</i> -Bu	
1b 4-MeC <sub>6</sub> H <sub>4</sub>	19%	1i Me	
1c Ph	26%	1j Ph	
1d 4-FC <sub>6</sub> H <sub>4</sub>	11%	1k H	
1e 4-CF <sub>3</sub> C <sub>6</sub> H <sub>4</sub>	13%	1l Cl	
1f 3,5-F <sub>2</sub> C <sub>6</sub> H <sub>3</sub>	n.d. <sup>b</sup>	1m CF <sub>3</sub>	
1g 3,5-Me <sub>2</sub> C <sub>6</sub> H <sub>3</sub>	21%		

<sup>a</sup>Yield over two steps from 6. <sup>b</sup>Insolubility of 1f prevented confirmation of purity and characterization.

Figure 1 outlines these steps, comprised of (1) reduction of the pyridinium 1 to give a neutral pyridyl radical 2, (2) possible oxidation of this neutral pyridyl radical (the reverse of the reduction), (3) cleavage of the C–N bond of the pyridyl radical 2 to release pyridine 4 and an alkyl radical, and (4) the potential recombination of pyridine 4 and alkyl radical to reconstitute the pyridyl radical 2. For these efforts, we deployed electrochemical measurements and DFT calculations to interrogate the factors controlling reactivity. In order to generate results that would advance the use of these reagents across multiple activation modes (metal catalysis, photoredox

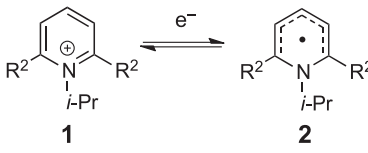
**Table 1.** Single-Electron Reduction of Pyridinium Salt **1** to Pyridyl Radical **2** (Figures 1 and 2)


entry	Ar	$\sigma^a$	$\Delta G_{\text{calc}}^0$ <sup>b</sup> (kcal/mol)		$\Delta G_{\text{exp}}^0$ <sup>c</sup> (kcal/mol)
			R <sup>1</sup> = <i>i</i> -Pr	R <sup>1</sup> = Cy	R <sup>1</sup> = Cy
1	4-MeOC <sub>6</sub> H <sub>4</sub> , <b>1a</b>	-0.27	9.2	9.5	8.4
2	4-MeC <sub>6</sub> H <sub>4</sub> , <b>1b</b>	-0.17	8.3	8.3	6.3
3	Ph, <b>1c</b>	0.00	5.9	6.1	5.0
4	4-FC <sub>6</sub> H <sub>4</sub> , <b>1d</b>	0.06	5.4	5.7	4.4
5	4-CF <sub>3</sub> C <sub>6</sub> H <sub>4</sub> , <b>1e</b>	0.54	0.8	0.4	0.0
6	3,5-F <sub>2</sub> C <sub>6</sub> H <sub>3</sub> , <b>1f</b>	0.68 <sup>d</sup>	0.0	0.0	nd <sup>e</sup>
7	3,5-Me <sub>2</sub> C <sub>6</sub> H <sub>3</sub> , <b>1g</b>	nd	7.6		6.8

<sup>a</sup>Hammett  $\sigma_p$  parameters<sup>14</sup> for substituents. <sup>b</sup>Relative Gibbs free energies computed using UM06/6-311+G(d,p), SMD: DMF//UB3LYP/6-31G(d). <sup>c</sup> $\Delta G_{\text{exp}}^0$  calculated using  $\Delta G_{\text{exp}}^0 = -FE_{\text{exp}}^0$ . <sup>d</sup>For 3,5-difluoro substitution, the  $\sigma$  parameter was estimated additively as a sum of two fluorine  $\sigma_m$  values of 0.34. <sup>e</sup>Insolubility of this pyridinium salt prevented accurate measurement of the reduction potential.

catalysis, and EDA photoactivation), electrochemical activation of the pyridiniums was examined. This mode eliminates variables associated with different catalytic conditions. This approach allowed us to dissect the thermodynamics of the first step (pyridinium salt to pyridyl radical; **1** → **2**) as well as the thermodynamics (**2** → **4**) and kinetics of step two (**2** → **3/4** → **3**).

We considered systems with several different substitutions of the pyridinium fragment. One class we investigated is 2,4,6-triarylpyridinium salts (Scheme 2B).<sup>13</sup> These 2,4,6-triarylpyridinium salts (**1a**-Cy–**1e**-Cy, **1g**-Cy) are easily synthesized by refluxing cyclohexyl amine with pyrylium **7**, which was generated from 2 equiv of an acetophenone (**5**) and 1 equiv of a benzaldehyde (**6**) (Scheme 2A). This protocol allows ready synthetic access such that comparison of experimental and computed reactivity data is possible. In our computational

**Table 2.** Single-Electron Reduction of Hypothetical Pyridinium Cations


entry	R <sup>2</sup>	$\sigma_p^a$	$\nu^a$	$\Delta G_{\text{red}}^0$ <sup>b</sup> (kcal/mol)
1	<i>t</i> -Bu, <b>1h</b>	-0.20	1.24	19.2
2	Me, <b>1i</b>	-0.17	0.52	34.2
3	Ph, <b>1j</b>	-0.01	0.57	24.5
4	H, <b>1k</b>	0.00	0.00	30.4
5	Cl, <b>1l</b>	0.23	0.55	15.6
6	CF <sub>3</sub> , <b>1m</b>	0.54	0.91	0.0

<sup>a</sup>Hammett sigma para ( $\sigma_p$ ) and Charton steric ( $\nu$ ) parameter<sup>15</sup> for the R groups. <sup>b</sup>Relative Gibbs free energies are computed with UM06/6-311+G(d,p), SMD: 1,4-dioxane//UB3LYP/6-31G(d).

studies, we considered both cyclohexyl and isopropyl groups at R<sup>1</sup> to confirm that cyclic and acyclic systems behaved similarly. We originally attempted to synthesize pyridinium **1f** with 3,5-difluorophenyl substitution. However, insolubility of **1f** prevented characterization and accurate measurement of its reduction potential. All further analysis of this compound was solely computational. Due to this difficulty, we prepared pyridinium salt **1g** as an additional data point to correlate the experimental and computed reduction potentials. In addition, a complementary set of hypothetical pyridinium salts were also subjected to computation (Scheme 2B). Substitution in these compounds is more diverse and includes groups that permit both electronic and steric differentiation that we could not easily synthesize. Because we saw good agreement between the cyclohexyl and isopropylpyridinium salts for **1a**–**1g**, we focused on the isopropylpyridiniums for **1h**–**1m**. The 4-aryl substituent was also removed from these hypothetical pyridinium salts to facilitate computation. Finally, pyridinium salt **1n**-Cy was used to determine the effect of the 2,6-aryl substituents on the reduction potential.

**Pyridinium Salt Reduction.** From the pyridinium, the first part of the amine activation is reduction of the pyridinium moiety. In assessing this reduction step, a relevant numerical

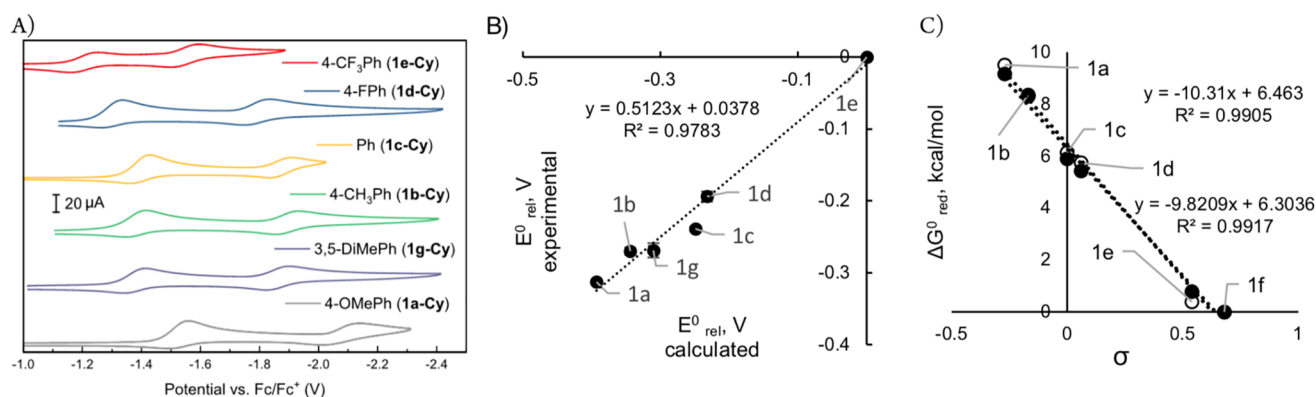
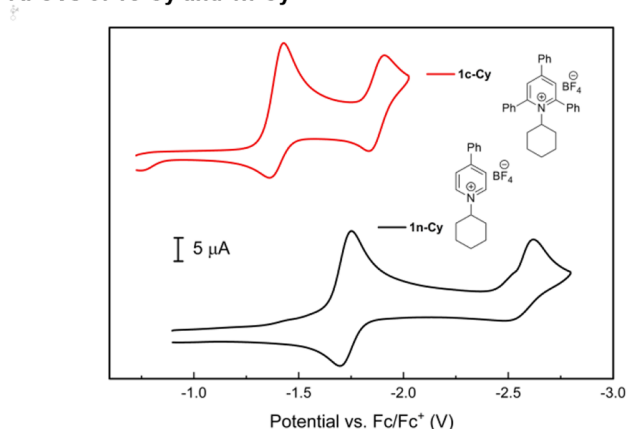
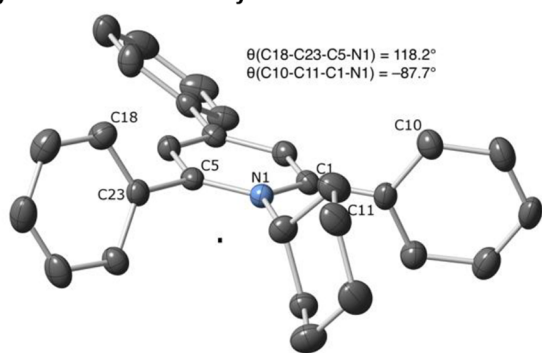


**Figure 2.** (A) Cyclic voltammograms recorded for the set of cyclohexylpyridinium salts **1a**–**1g** listed in Table 1. CVs were recorded under a N<sub>2</sub> atmosphere using a glassy carbon working electrode at a scan rate of 100 mV/s. Potentials are reported versus an internal Fc/Fc<sup>+</sup> reference. (B) Experimentally determined relative reduction potentials of pyridinium salts vs corresponding DFT-computed values from Table 1. (C) Relative Gibbs free energy of single-electron reduction for a set of pyridinium cations vs Hammett parameters from Table 1. Black and white markers represent N-*i*-Pr and N-Cy, respectively.

## A. CVs of 1c-Cy and 1n-Cy



## B. Crystal Structure of 1c-Cy



## C. Crystal Structure of 1c-iPr

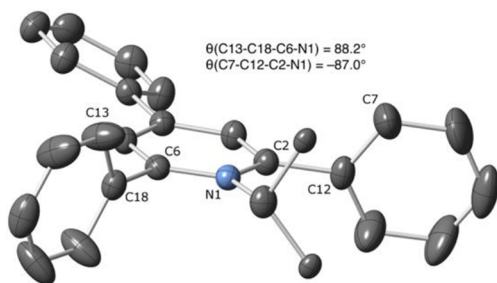


**Figure 3.** (A) CVs recorded for 2,4,6-triphenylcyclohexyl pyridinium salt **1c-Cy** and 4-phenyl-cyclohexyl pyridinium salt **1n-Cy** under a  $N_2$  atmosphere using a glassy carbon working electrode at a scan rate of 100 mV/s. Potentials are reported versus an internal  $Fc/Fc^+$  reference. (B) Molecular diagram of **1c-Cy** with ellipsoids at 50% probability. H-atoms and  $BF_4^-$  omitted for clarity. (C) Molecular diagram of **1c-iPr** with ellipsoids at 50% probability. H-atoms,  $BF_4^-$ , and disorder omitted for clarity.

measure would be the thermodynamic stability of the pyridyl radical **2** relative to the corresponding pyridinium cation **1**. The relative Gibbs free energies ( $\Delta G_{\text{calc}}^0$ ) were computed using UM06/6-311+G(d,p), SMD: DMF//UB3LYP/6-31G(d), and the values listed are relative to the most readily reduced pyridinium salt **1f** (Table 1).

The reduction potentials of cyclohexylpyridinium salts were also measured experimentally by recording the cyclic voltammograms (CVs) shown in Figure 2A. Because the redox waves for the pyridinium derivatives surveyed in Figure 2A show varying levels of reversibility, we also employed differential pulse voltammetry (DPV) to provide an alternative

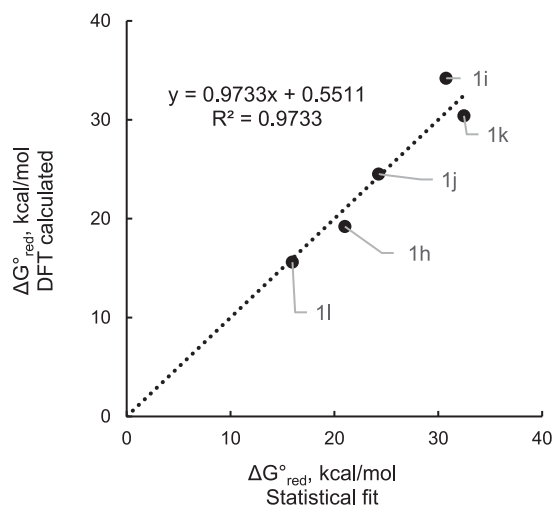


**Figure 4.** Relative Gibbs free energy of single-electron reduction for a set of the hypothetical *N*-*i*-Pr pyridinium cations **1h–1m**. DFT-computed values vs those calculated via multilinear regression (eq 2).

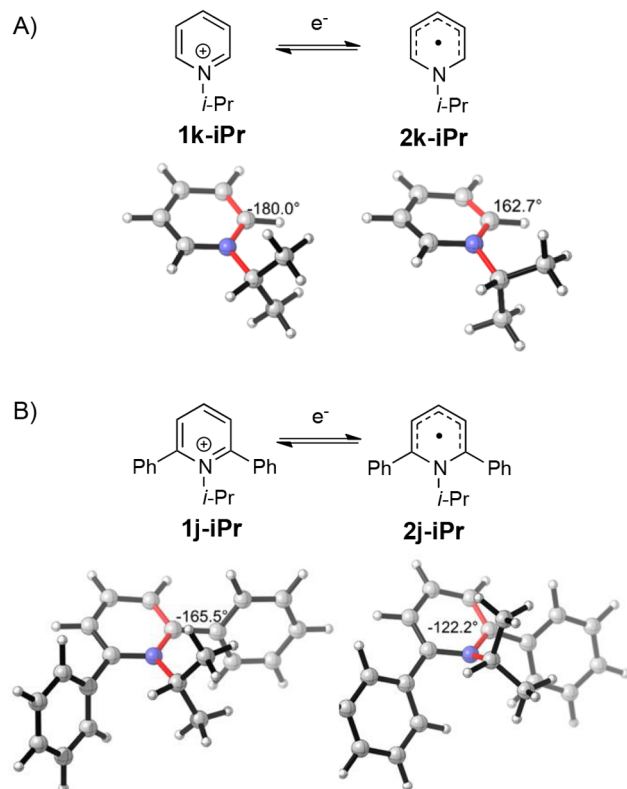


**Figure 5.** (A) Distortion of the unsubstituted pyridinium cation **1k-iPr** upon reduction to **2k-iPr**. (B) Distortion of the diphenyl substituted pyridinium cation **1j-iPr** upon reduction to **2j-iPr**. Values of the dihedral angle (degrees) for the bonds highlighted in red are shown. Optimizations were performed using UB3LYP/6-31G(d). Optimizations using explicit, and implicit solvation did not produce significantly different results.

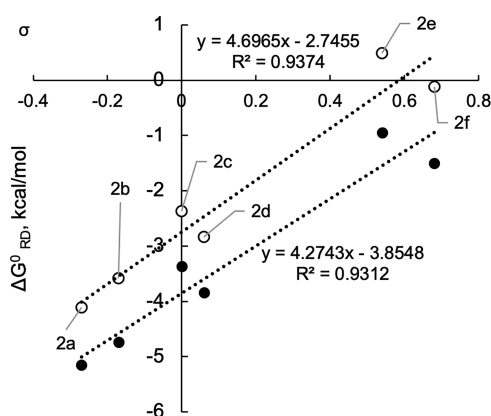
measure of the potentials at which the cyclohexylpyridinium salts are reduced in anhydrous DMF containing 0.1 M TBAPF<sub>6</sub> as supporting electrolyte. Relative redox potentials ( $E_{\text{rel}}^0$ ) recorded by DPV (see the Supporting Information) were calibrated against an internal ferrocene standard and were



**Table 3. Thermodynamics of Dissociation of the Pyridyl Radical**

entry	Ar	$\sigma^a$	$\Delta G_{RD}^0$ (kcal/mol)	
			$R^1 = \text{Cy}$	$R^1 = i\text{-Pr}$
1	4-MeOC <sub>6</sub> H <sub>4</sub> , <b>2a</b>	−0.27	−4.1	−5.2
2	4-MeC <sub>6</sub> H <sub>4</sub> , <b>2b</b>	−0.17	−3.6	−4.7
3	Ph, <b>2c</b>	0.00	−2.4	−3.4
4	4-FC <sub>6</sub> H <sub>4</sub> , <b>2d</b>	0.06	−2.8	−3.8
5	4-CF <sub>3</sub> C <sub>6</sub> H <sub>4</sub> , <b>2e</b>	0.54	0.5	−0.9
6	3,5-F <sub>2</sub> C <sub>6</sub> H <sub>3</sub> , <b>2f</b>	0.68	−0.1	−1.5

<sup>a</sup>Hammett  $\sigma_p$  parameters for the aryl substituents. <sup>b</sup>Gibbs free energies for dissociation are computed using UM06/6-311+G(d,p), SMD: DMF//UB3LYP/6-31G(d).

**Figure 6.** Gibbs free energies for radical dissociation of the pyridyl radical vs Hammett parameters. Data from Table 3. Black and white markers represent *N*-*i*-Pr and *N*-Cy, respectively.**Table 4. Free Energies for the Radical Dissociation of Hypothetical Systems**

entry	R <sup>2</sup>	$\sigma^a$	$\nu^a$	$\Delta G_{RD}^0$ (kcal/mol)
1	<i>t</i> -Bu, <b>2h</b>	−0.20	1.24	−23.1
2	Me, <b>2i</b>	−0.17	0.52	−11.4
3	Ph, <b>2j</b>	−0.01	0.57	−5.1
4	H, <b>2k</b>	0.00	0.00	1.2
5	Cl, <b>2l</b>	0.23	0.55	−8.0
6	CF <sub>3</sub> , <b>2m</b>	0.54	0.91	−9.0

<sup>a</sup>Hammett sigma para ( $\sigma_p$ ) and Charton steric ( $\nu$ ) parameters<sup>3</sup> for the R groups. <sup>b</sup>Values are obtained using UM06/6-311+G(d,p), SMD: 1,4-dioxane//UB3LYP/6-31G(d).

converted to the relative thermodynamics of the reduction using eq 1 (where  $n = 1$ ).

$$\Delta G_{\text{red}}^0 = -nFE_{\text{red}}^0 \quad (1)$$

The computationally determined reduction potentials of the *N*-Cy pyridinium salts were compared to the values determined experimentally by DPV (Table 1). Strong agreement between the computational and experimental data indicates that we appropriately capture the reactivity of the salts in the reduction step, confirming the suitability of the chosen level of theory (Figure 2B). The computational and experimental data indicates that more electron-rich systems are more difficult to reduce. A strong Hammett correlation is observed for both *N*-Cy and *N*-*i*-Pr systems upon plotting  $\Delta G_{\text{red}}^0$  vs  $\sigma$  (Figure 2C).<sup>14</sup> Both *N*-Cy and *N*-*i*-Pr systems exhibit near identical behavior and are equally sensitive to the electronic character of the aryl groups, as reflected in the similar values of the linear fitting coefficients.

The relative free energies of the reduction were computed for a series with differing 2,6-substitution (Table 2). Notably, these calculations reproduce the trend in Figure 3A with 2,6-diphenyl substitution facilitating reduction (entries 3 vs 4). Similar to our experimental results, electron-withdrawing groups show a shift to more positive reduction potentials (entries 4 vs 5 and 6). An unexpected steric effect was also observed. When groups with similar Hammett parameters were compared, a lower reduction potential was observed with larger 2,6-substituents (entries 1 vs 2). These trends suggest that steric strain facilitates SET by destabilizing the pyridinium salt. These substituent effects work synergistically; groups that possess both steric bulk and electron-withdrawing properties minimize the reduction potential (entry 6).

As we were examining the electrochemical reductions of these alkylpyridinium salts, we observed that compound **1n-Cy**, lacking the 2,6-diphenyl groups, was harder to reduce than the parent 2,4,6-triphenylpyridinium **1c-Cy** (Figure 3A). Because the crystal structure of **1c-Cy** and *i*-Pr variant **1c-*i*Pr** showed little conjugation between the 2,6-aryl groups and the pyridinium ring (Figure 3B,C), we set out to interrogate whether this difference was due primarily to steric or electronic effects.

To probe the relative importance of these effects, the calculated reduction potentials were subjected to a multilinear regression analysis using Hammett ( $\sigma_p$ ) and Charton ( $\nu$ )<sup>15</sup> parameters of the 2,6-substituents ( $R^2$ ) as independent variables. For this system, the following correlation in eq 2 was obtained. The statistical model is in excellent agreement with DFT-calculated values across the entire range of free energies (Figure 4). The negative values of the coefficients indicate that electron-withdrawing groups and large steric groups facilitate reduction. The larger absolute value of the coefficient for  $\sigma_p$  vs  $\nu$  highlights that electronic effects are more pronounced in this series.<sup>16</sup>

$$\Delta G_{\text{red}}^0 = -35.87\sigma_p - 15.03\nu + 32.48 \quad (2)$$

The electronic effect is consistent with electron-withdrawing groups facilitating uptake of an electron, but the steric impact on the reduction potential was not obvious. To interrogate the origin of this steric effect, the computed structures of pyridinium cations and their corresponding radicals were analyzed (Figure 5).

To maintain aromaticity, the starting pyridinium systems tend to be as flat as possible; however, with the 2,6-diphenyl groups, the isopropyl is forced out of the pyridinium plane by approximately 15° (180° in **1k-*i*Pr** vs 165.5° in **1j-*i*Pr**). On the other hand, the pyridyl radical contains seven electrons in the

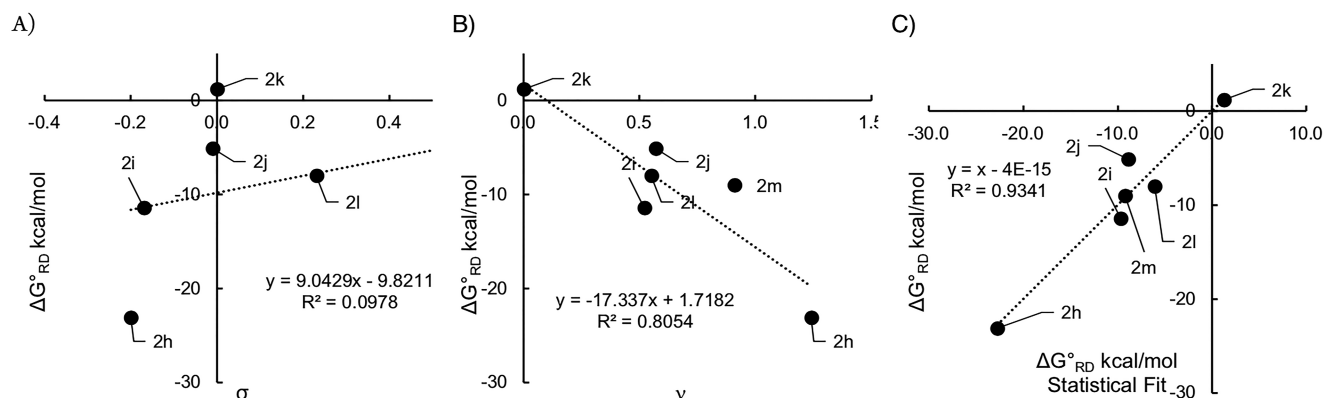


**Figure 7.** Gibbs free energies for radical dissociation of a set of the hypothetical *N*-*i*-Pr pyridyl radicals **2h**–**2m**. Data from Table 4. (A) Vs Hammett parameters. (B) Vs Charton parameters. (C) Vs Hammett and Charton parameters.

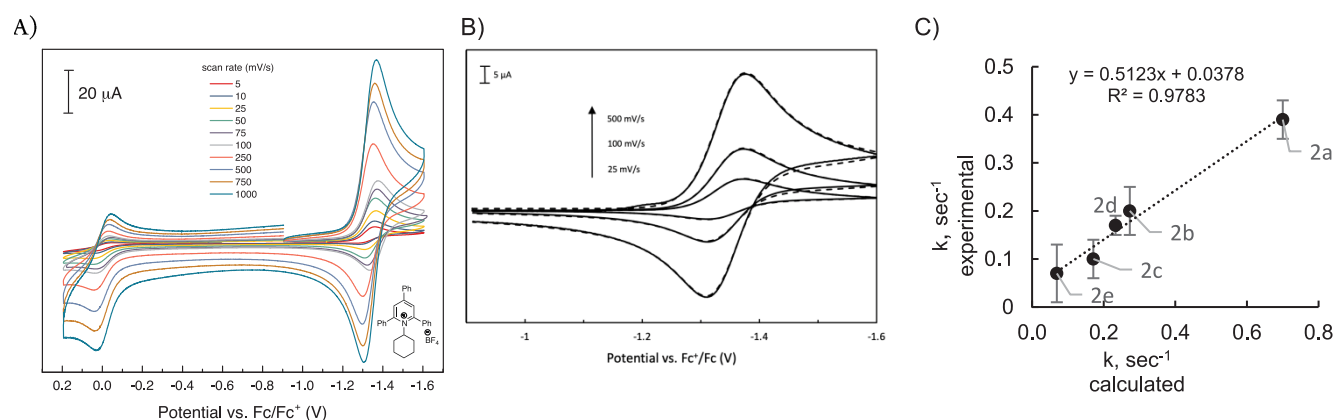


**Figure 8.** (A) Scan rate studies of the first reduction wave for pyridinium salt **1c-Cy**. (B) Experimental (solid) vs simulated (dashed) data of **1c-Cy** first reduction at different scan rates. Simulation parameters:  $E^0 = -1.34$  V vs  $\text{Fc}^+/\text{Fc}$ ,  $k_s = 0.05$  cm s<sup>-1</sup>,  $k_f = 0.01$  s<sup>-1</sup>. (C) Experimentally determined rate constants of radical dissociation of **2** vs DFT-computed values.

six-membered ring and is no longer fully aromatic. As a consequence, the nitrogen adopts a configuration intermediate between  $\text{sp}^2$  and  $\text{sp}^3$  (dihedral angle =  $162.7^\circ$  in **2k-iPr** vs  $180^\circ$  in **1k-iPr**). Notably, 2,6-disubstitution amplifies this effect ( $122.2^\circ$  in **2j-iPr** vs  $162.7^\circ$  in **2k-iPr**), allowing the steric clash between the isopropyl and phenyl groups to be alleviated. Pyramidalization values (see the Supporting Information; sum of bond angles around the nitrogen atom; planar =  $360^\circ$ ) also indicate deviation from planarity in both systems as well as more significant distortion in 2,6-disubstituted systems ( $347.8^\circ$  for **2j-iPr** vs  $356.5^\circ$  for **2k-iPr**). Importantly, this increased  $\text{sp}^3$  character on nitrogen weakens the C–N bond and preorganizes the pyridyl radical for C–N bond cleavage as the overlap between C–N  $\sigma^*$  and the pyridyl  $\pi$ -orbital gets larger.

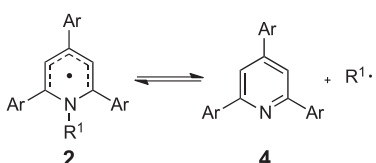
**C–N Bond Cleavage.** With the stage set by reduction to form the alkyl radical by dissociation, we turned to examination of the substituent effects on the thermodynamic and kinetic aspects of this homolytic bond cleavage process. In addition to the changes in reduction potential discussed above, we also observed that varying the substitution of the pyridinium salt correlates with variable extents of redox reversibility, as can be noted by inspection of the CV traces in Figure 2A. This variability suggested to us that slow chemical steps may be linked to the electrochemical reduction

steps revealed through the voltammetry (i.e., EC reaction pathways).

To understand these effects on the thermodynamics of this dissociation step, we turned to a computational approach. With respect to electronic effects on the thermodynamics of radical dissociation, we observed that electron-donating substituents substantially favored radical dissociation (Table 3). Indeed, a plot of calculated Gibbs free energies of dissociation against the Hammett parameters of substituents indicates a moderately strong ( $\rho = 4.3, 4.7$ ) positive Hammett correlation (Figure 6). For both *N*-*i*-Pr and *N*-Cy systems, the magnitude of the electronic effect is smaller than in the preceding SET step. As shown in Figure 5B, the nitrogen lone pair in the radical is still partially conjugated with the  $\pi$ -system. There is a net decrease in the  $\pi$ -electron density to only six electrons upon radical dissociation. Thus, electron donors would be expected to favor dissociation due to a formal decrease in  $\pi$ -electron density.

In the above series, the phenyl groups at the 2,6-positions have similar steric features. To estimate to what degree changing the steric bulk at these positions would change the overall thermodynamics, the free energy of radical dissociation was computed for a series of hypothetical 2,6-substituted pyridyl radicals (Table 4). A pronounced dependence between the thermodynamics and the size of the R<sup>2</sup> groups is observed. Indeed, there is a good linear relationship between the radical

**Table 5. Activation Free Energies for the Radical Dissociation of Pyridyl Radical 2 to Pyridine 4 (Figures 1 and 2)**



entry	Ar	$\sigma^a$	calc $\Delta G_{RD}^\ddagger$ <sup>b</sup> (kcal/mol)		expt $\Delta G_{RD}^\ddagger$ <sup>c</sup> (kcal/mol)
			R <sup>1</sup> = <i>i</i> -Pr	R <sup>1</sup> = Cy	R <sup>1</sup> = Cy
1	4-MeOC <sub>6</sub> H <sub>4</sub> , <b>2a</b>	−0.27	15.9	17.7	18.0
2	4-MeC <sub>6</sub> H <sub>4</sub> , <b>2b</b>	−0.17	16.5	18.2	18.4
3	Ph, <b>2c</b>	0.00	17.3	18.5	18.8
4	4-FC <sub>6</sub> H <sub>4</sub> , <b>2d</b>	0.06	16.9	18.3	18.5
5	4-CF <sub>3</sub> C <sub>6</sub> H <sub>4</sub> , <b>2e</b>	0.54	17.5	19.0	19.0
6	3,5-F <sub>2</sub> C <sub>6</sub> H <sub>3</sub> , <b>2f</b>	0.68 <sup>d</sup>	17.4	19.1	nd <sup>e</sup>
7	3,5-Me <sub>2</sub> C <sub>6</sub> H <sub>3</sub> , <b>2g</b>	nd	nd	nd	18.7

<sup>a</sup>Hammett  $\sigma_p$  parameters for substituents. <sup>b</sup>Gibbs free energies of activation computed using UM06/6-311+G(d,p), SMD: DMF//UB3LYP/6-31G(d). <sup>c</sup>Experimental  $\Delta G_{RD}^\ddagger$  obtained from rate constants using the Eyring equation. <sup>d</sup>For 3,5-difluoro substitution, the  $\sigma$  parameter was estimated additively as a sum of two fluorine  $\sigma_m$  values of 0.34. <sup>e</sup>Insolubility of this pyridinium salt prevented accurate measurement.

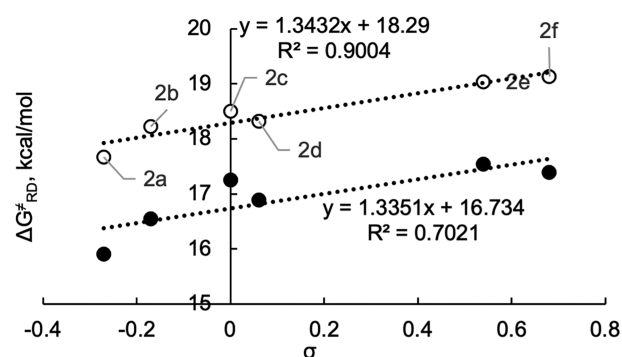
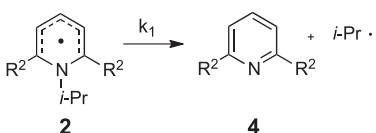


**Figure 9.** Activation free energy of radical dissociation for a set of pyridinium cations vs Hammett parameters. Data from Table 5. Black and white markers represent *N*-*i*-Pr and *N*-Cy, respectively.

**Table 6. Activation Free Energies for the Radical Dissociation of Hypothetical Systems**



entry	R <sup>2</sup>	$\sigma^a$	$\nu^a$	$\Delta G_{RD}^\ddagger$ <sup>b</sup> (kcal/mol)
1	<i>t</i> -Bu, <b>2h</b>	−0.20	1.24	11.4
2	Me, <b>2i</b>	−0.17	0.52	15.0
3	Ph, <b>2j</b>	−0.01	0.57	15.5
4	H, <b>2k</b>	0.00	0.00	22.3
5	Cl, <b>2l</b>	0.23	0.55	12.7
6	CF <sub>3</sub> , <b>2m</b>	0.54	0.91	13.6

<sup>a</sup>Hammett sigma para ( $\sigma_p$ ) and Charton steric ( $\nu$ ) parameters<sup>3</sup> for the R groups. <sup>b</sup>Values are obtained using UM06/6-311+G(d,p), 4SMD: 1,4-dioxane//UB3LYP/6-31G(d).

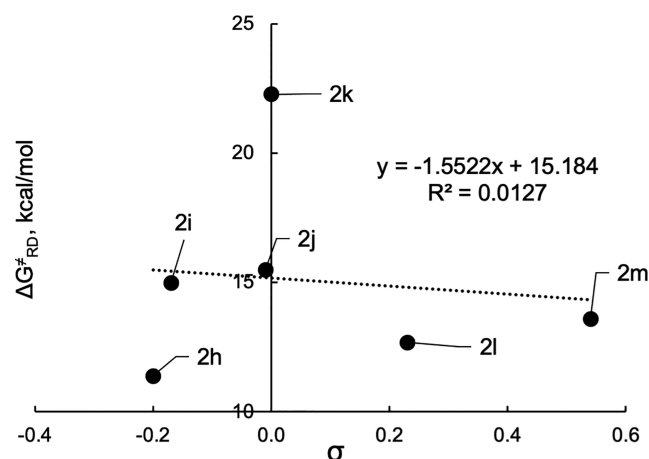


**Figure 10.** Activation free energy of radical dissociation for a set of model pyridyl radicals **2h–2m** vs Hammett parameters. Data from Table 6.

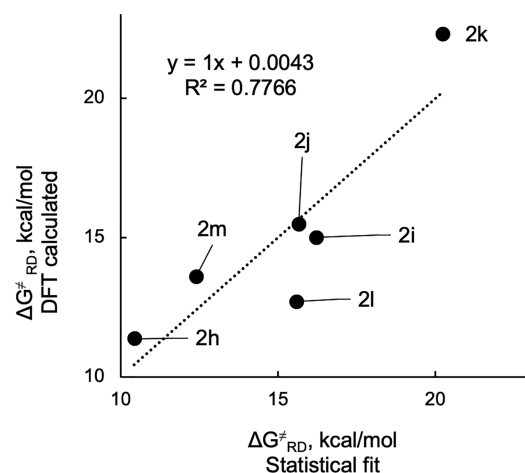
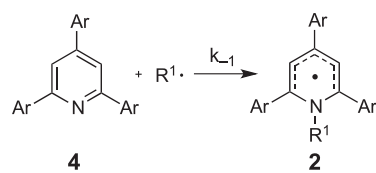


**Figure 11.** Activation free energy of radical dissociation for a set of the hypothetical pyridyl radicals **2h–2m** vs those calculated via multilinear regression (eq 4). Data from Table 6.

**Table 7. Activation Free Energies for the Attack of Alkyl Radicals on Neutral Pyridines**



entry	Ar	$\sigma^a$	$\Delta G_{RA}^\ddagger$ <sup>b</sup> (kcal/mol)	
			R <sup>1</sup> = Cy	R <sup>1</sup> = <i>i</i> -Pr
1	4-MeOC <sub>6</sub> H <sub>4</sub> , <b>4a</b>	−0.27	21.8	21.1
2	4-MeC <sub>6</sub> H <sub>4</sub> , <b>4b</b>	−0.17	21.8	21.3
3	Ph, <b>4c</b>	0.00	20.9	20.6
4	4-FC <sub>6</sub> H <sub>4</sub> , <b>4d</b>	0.06	21.1	20.7
5	4-CF <sub>3</sub> C <sub>6</sub> H <sub>4</sub> , <b>4e</b>	0.54	18.6	18.5
6	3,5-F <sub>2</sub> C <sub>6</sub> H <sub>3</sub> , <b>4f</b>	0.68	19.2	18.9

<sup>a</sup>Hammett  $\sigma_p$  parameters for substituents. <sup>b</sup>Values are obtained using UM06/6-311+G(d,p), SMD: DMF//UB3LYP/6-31G(d).

dissociation free energies and the Charton values of the R<sup>2</sup> groups (Figure 7B). This steric effect is readily rationalized; as the R<sup>1</sup> group dissociates, unfavorable steric interactions with

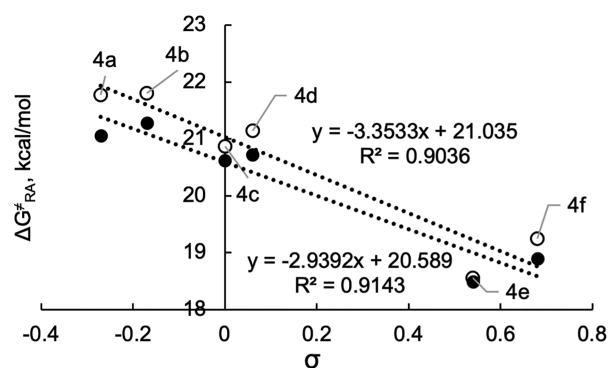


**Figure 12.** Activation free energy of a radical attack for a set of pyridinium cations vs Hammett parameters. Data from Table 7. Black and white markers represent *N*-Cy and *N*-*i*-Pr, respectively.

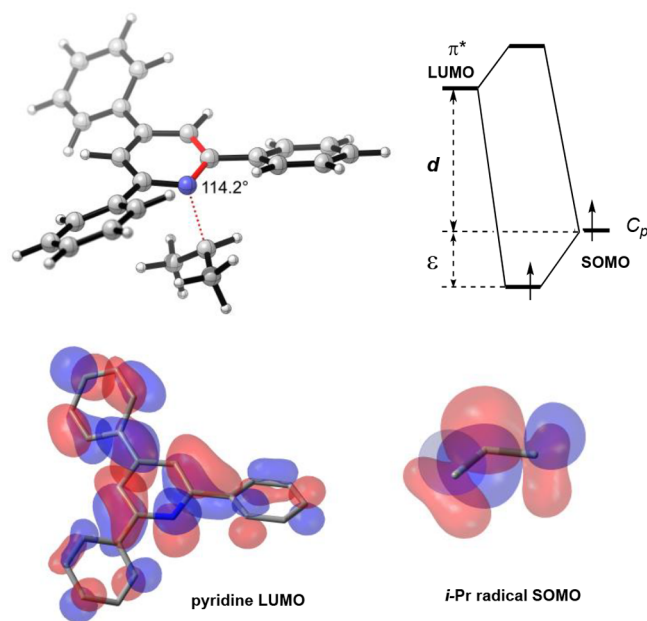


**Figure 13.** Example of the radical dissociation transition state and corresponding MO interaction diagram. The energetic effect of the overlap is  $\epsilon$ ; the initial energy SOMO–LUMO gap is  $d$ .

the  $R^2$  substituents are eliminated. On the other hand, a plot of  $\sigma$  vs  $\Delta G^0$  suggests that there is no apparent correlation in this series with the  $R^2$  electronic character ( $\sigma$ , Figure 7A). However, a multilinear regression reveals that both factors contribute to the variance (Figure 7C, eq 3) with normalized values showing that the electronic parameter contributes to ~25% of the variance and the steric parameter accounts for the majority of the variance at ~75% (see the Supporting Information):

$$\Delta G_{RD}^0 = 10.38\sigma_p - 17.68\nu + 1.27 \quad (3)$$

Having evaluated the thermodynamics, the kinetics of the dissociation step were next considered. The lack of full reversibility in the reduction of the pyridinium salts provides the opportunity to extract the rate of the pyridyl radical decomposition through analysis of the pyridinium CVs. To quantitate how pyridinium structure and substitution patterns influence this reversibility, CVs for each of the pyridinium salts of Table 1 were recorded at varying scan rates (5–1000 mV/s) to assess how electrode dynamics and the kinetics of possible

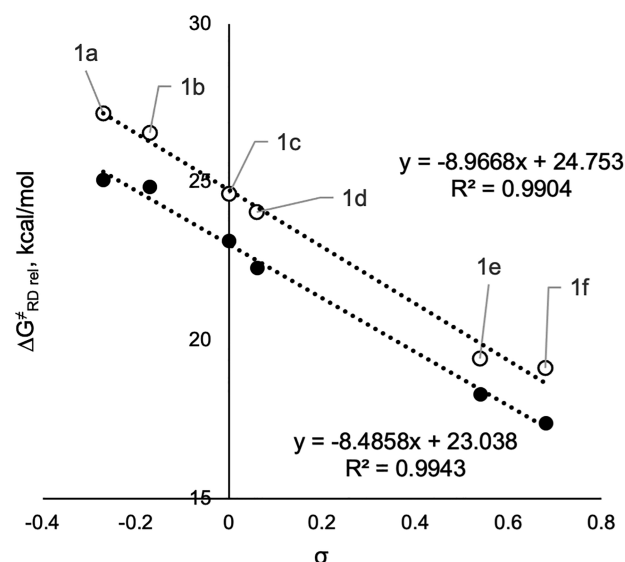


**Figure 14.** Relative activation free energy of radical dissociation for pyridinium systems vs Hammett parameters. Note that the values of relative activation free energies were obtained using *relative*  $\Delta G_{RD}^0$  (see Table 1) via  $\Delta G_{RD,rel}^\ddagger = \Delta G_{RD}^0 + \Delta G_{RD}^\ddagger$ . Absolute values of  $\Delta G_{RD,rel}^\ddagger$  will depend on the exact nature of the reductant used. Black and white markers represent *N*-*i*-Pr and *N*-Cy, respectively.

chemical steps may influence the shape of CV traces (results obtained for 1c-Cy are shown as an example in Figure 8A). Through simulations of an EC reaction scheme involving an initial electrochemical step (i.e., pyridinium reduction) followed by a chemical step (i.e., pyridyl radical dissociation/C–N bond scission), we were able to reproduce the CVs with high fidelity (Figure 8B) and extract the amalgamated rate constants. Computation of the radical dissociation of pyridyl radicals derived from 1a–1g gave rise to activation free energies that could be converted to  $k_{RD}$  values. These values correlated strongly to those determined through CV simulations (see Figure 8C, Table 5).

The activation energy of the radical dissociation is much less affected by the electronics of the pyridinium system ( $\rho = +1.3$ ,  $+1.3$ ; Figure 9) compared to the thermodynamics of radical dissociation ( $\rho = +4.2$ ,  $+4.7$ ; Figure 6).

Since all of these substrates had aryl substituents of very similar steric bulk flanking the alkyl group that departs as a radical, we turned to computation to better understand steric nuances of these systems. In doing so, it appears that the weak electronic effects of substituents can be completely overridden by steric effects, as shown by analysis of activation energies for the model systems (Table 6). Namely, larger  $R^2$  groups lower the dissociation barrier. For these model systems, there is no pronounced dependence of the dissociation activation energy on the electronics of the  $R^2$  groups (Figure 10). As with the thermodynamics, multilinear regression incorporating both the Hammett and Charton parameters reveals the strongest correlation (Figure 11). The majority of the variance is found in the Charton steric parameter, as indicated by the larger coefficient in eq 4.<sup>17</sup>

$$\Delta G_{RD}^\ddagger = -0.79\sigma_p - 6.54\nu + 18.91 \quad (4)$$

To gain insight into the orbital basis for these substituent effects, it is instructive to examine the kinetics of the reverse



reaction, specifically the radical association with the neutral pyridine (Table 7). As would be expected from the relationship

$$\Delta G_{\text{RA}}^{\ddagger} = \Delta G_{\text{RD}}^{\ddagger} + (-\Delta G_{\text{RD}}^0) \quad (5)$$

the electronic effects in radical association can be approximated by those from radical dissociation barriers ( $\rho = +1.3$ ,  $+1.3$ ; Figure 9) subtracted by those from the thermodynamics ( $\rho = +4.2$ ,  $+4.7$ ; Figure 6). Indeed, this relationship largely holds, as shown in Figure 12 ( $\rho = -2.9$ ,  $-3.4$ ). Specifically, electron-withdrawing groups accelerate radical association, while electron-donating groups strongly favor the dissociation thermodynamically and weakly accelerate the dissociation kinetically.

Examination of the frontier molecular orbitals interacting during the process provides insight into these electronic effects. Positioning of the alkyl group almost perpendicular to the plane of the pyridine ring in the transition state suggests that there is a key interaction between the SOMO of a radical and the LUMO of a pyridine (Figure 13). The energetic effect of the overlap is inversely proportional to the initial energy separation  $d$ .<sup>18</sup> Electron-withdrawing groups in a pyridine system lower the LUMO energy, decreasing the LUMO–SOMO gap ( $d$  on the diagram), thus enhancing the interaction and stabilizing the corresponding association transition state. This relationship also suggests that electron-rich radicals should be more reactive in the association process.

**Overall Effects on Reduction and C–N Bond Cleavage.** A specific approach to the design of the pyridinium moiety for the C–N bond activation depends on the type of reduction of pyridinium salts. If reduction of the salt is performed in a fashion orthogonal to the further thermal chemical reaction (i.e., electrochemical or photochemical generation of pyridyl radicals), then the reactivity of the compound in C–N homolytic bond cleavage is determined only by the corresponding radical dissociation activation energy ( $\Delta G_{\text{RD}}^{\ddagger}$  on Figure 1). In this case, bulky and electron-rich pyridine groups will facilitate the activation. Based on our study, it appears that the electronic character of the pyridine moiety has only a minor effect in this case.

However, if reduction contributes to the overall thermal chemical transformation, then the rate of activation is controlled by the dissociation transition state energy *relative to the pyridinium* ( $\Delta G_{\text{RD,rel}}^{\ddagger}$  in Figure 1). Thus, one should consider electronic and steric effects over the sequence of reduction and dissociation steps. Because the activation energy of the dissociation step is weakly favored by electron-donating substituents and reduction is heavily favored by electron-withdrawing substituents, it should be possible to accelerate the overall process using electron-withdrawing substituents. Indeed, a Hammett correlation using  $\Delta G_{\text{RD,rel}}^{\ddagger}$  reveals a large negative  $\rho$  value (Figure 14). The electronic effects are very pronounced and must be accounted for accordingly in design of any process. Notably, this correlation is the strongest we have observed, likely because the relative energy of the pyridyl radical **2** can either be higher or lower than that of the pyridinium cation, obfuscating the dependence of individual steps on the electronics and sterics (Figure 1). It is the overall transition state barrier from the pyridinium cation (**1**) to the radical dissociation transition state (**3**) that is key to understanding these systems.

## CONCLUSIONS

In summary, this analysis reveals the fundamental trends affecting the individual steps as well as the overall process

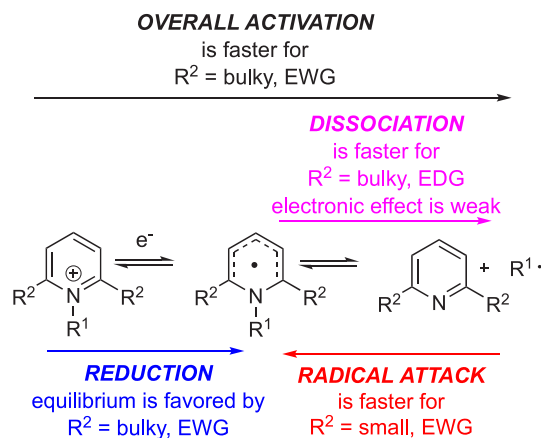


**Figure 15.** Computationally identified reactivity trends for substituted N-alkylpyridinium salts.

(Figure 15). The predominant control factor in the reduction of the pyridinium cation is electronic in nature, which could arise from substituents at any position of the pyridinium ring. A somewhat lesser dependence on steric factors is seen with larger groups at the 2,6-positions favoring reduction. On the other hand, the dissociation step exhibits a weak electronic dependence with electron-donating groups at any position of the pyridinium ring favoring dissociation. The influence of sterics on this step is very strong and easily outweighs the electronic influence, with large groups at the 2,6-positions favoring and accelerating dissociation. With respect to the overall process from the pyridinium cation to the alkyl radical, the electronic effects cancel, leading to more facile overall activation with electron-withdrawing groups. On the other hand, the steric effects are synergistic with larger groups promoting both steps and the overall process. Because the reduction is fast, emphasis should be placed on derivatives that promote dissociation to generate the alkyl radical. This knowledge creates a framework to enable the design of new pyridinium salts to meet the limitations that each mode of activation—transition metal catalysis, photoredox catalysis, or photoactivation via EDA complexes—currently encompasses.

## ASSOCIATED CONTENT

### Supporting Information

The Supporting Information is available free of charge at <https://pubs.acs.org/doi/10.1021/acscatal.1c01860>.

Experimental procedures and spectral data (PDF)

X-ray data for compounds **1c-Cy** and **1c-iPr** (CIF)

Primary NMR FID files, for compounds **1a-Cy**–**1e-Cy** and **1g-Cy** (ZIP)

## AUTHOR INFORMATION

### Corresponding Authors

Joel Rosenthal – Department of Chemistry and Biochemistry, University of Delaware, Newark, Delaware 19716, United States; [orcid.org/0000-0002-6814-6503](https://orcid.org/0000-0002-6814-6503); Email: [joelr@udel.edu](mailto:joelr@udel.edu)

Mary P. Watson – Department of Chemistry and Biochemistry, University of Delaware, Newark, Delaware 19716, United States; [orcid.org/0000-0002-1879-5257](https://orcid.org/0000-0002-1879-5257); Email: [mpwatson@udel.edu](mailto:mpwatson@udel.edu)

Marisa C. Kozlowski – Department of Chemistry, Roy and Diana Vagelos Laboratories, University of Pennsylvania, Philadelphia, Pennsylvania 19104, United States; [orcid.org/0000-0002-4225-7125](https://orcid.org/0000-0002-4225-7125); Email: [marisa@sas.upenn.edu](mailto:marisa@sas.upenn.edu)

## Authors

Sergei Tcyrlunikov – Department of Chemistry, Roy and Diana Vagelos Laboratories, University of Pennsylvania, Philadelphia, Pennsylvania 19104, United States

Qiuqi Cai – Department of Chemistry and Biochemistry, University of Delaware, Newark, Delaware 19716, United States

J. Cameron Twitty – Department of Chemistry and Biochemistry, University of Delaware, Newark, Delaware 19716, United States; [orcid.org/0000-0001-9524-1226](https://orcid.org/0000-0001-9524-1226)

Jianyu Xu – Department of Chemistry and Biochemistry, University of Delaware, Newark, Delaware 19716, United States

Abderrahman Atifi – Department of Chemistry and Biochemistry, University of Delaware, Newark, Delaware 19716, United States; [orcid.org/0000-0002-0163-5660](https://orcid.org/0000-0002-0163-5660)

Olivia P. Bercher – Department of Chemistry and Biochemistry, University of Delaware, Newark, Delaware 19716, United States

Glenn P. A. Yap – Department of Chemistry and Biochemistry, University of Delaware, Newark, Delaware 19716, United States

Complete contact information is available at: <https://pubs.acs.org/10.1021/acscatal.1c01860>

## Notes

The authors declare no competing financial interest.

## ACKNOWLEDGMENTS

M.C.K. thanks the NIH (R35 GM131902) for financial support and XSEDE (TG-CHE120052) for computational support. M.P.W. thanks the NIH (R35 GM131816) for financial support. J.C.T. thanks the Chemistry-Biology Interface program (NIH T32-GM133395). J.R. thanks the U.S. Department of Energy, Office of Science, Office of Basic Energy Sciences EPSCoR and Catalysis programs under Award Number DESC-0001234. Data were acquired at UD on instruments obtained with assistance of NSF and NIH funding (NSF CHE0421224, CHE1229234, CHE0840401, and CHE1048367; NIH P20 GM104316, P20 GM103541, and S10 OD016267).

## REFERENCES

- (1) A search of Pfizer's internal chemical store revealed over 47,000 alkyl primary amines vs about 28,000 primary and secondary alkyl halides: Garnsey, M. R. Pfizer Worldwide Research and Development, 2018.
- (2) For alkyl-NH<sub>2</sub> (1° and 2°), 1237920; data from the eMolecules Database accessed via REAXYS (April 8, 2019).
- (3) (a) Lawrence, S. A. *Amines: Synthesis, Properties and Applications*; Cambridge University Press: New York, 2004. (b) Nugent, T. C. *Chiral Amine Synthesis*; Wiley-VCH Verlag GmbH & Co. KGaA: Weinheim, Germany, 2010. (c) Ruiz-Castillo, P.; Buchwald, S. L. Applications of Palladium-Catalyzed C–N Cross-Coupling Reactions.

*Chem. Rev.* **2016**, *116* (19), 12564–12649. (d) McGrath, N. A.; Brichacek, M.; Njardarson, J. T. A Graphical Journey of Innovative Organic Architectures That Have Improved Our Lives. *J. Chem. Educ.* **2010**, *87* (12), 1348–1349. (e) Liu, Y.; Ge, H. Site-selective C–H arylation of primary aliphatic amines enabled by a catalytic transient directing group. *Nat. Chem.* **2017**, *9* (1), 26–32.

(4) (a) Ouyang, K.; Hao, W.; Zhang, W. X.; Xi, Z. Transition-Metal-Catalyzed Cleavage of C–N Single Bonds. *Chem. Rev.* **2015**, *115* (21), 12045–12090. (b) Pound, S. M.; Watson, M. P. Asymmetric Synthesis via Stereospecific C–N and C–O Bond Activation of Alkyl Amine and Alcohol Derivatives. *Chem. Commun.* **2018**, *54* (87), 12286–12301. (c) Xu, J.; Bercher, O. P.; Talley, M. R.; Watson, M. P. Nickel-Catalyzed, Stereospecific C–C and C–B Cross-Couplings via C–N and C–O Bond Activation. *ACS Catal.* **2021**, *11* (3), 1604–1612. (d) Li, M.-B.; Wang, Y.; Tian, S.-K. Regioselective and Stereospecific Cross-Coupling of Primary Allylic Amines with Boronic Acids and Boronates through Palladium-Catalyzed C–N Bond Cleavage. *Angew. Chem., Int. Ed.* **2012**, *51* (12), 2968–2971. (e) Moragas, T.; Gaydou, M.; Martin, R. Nickel-Catalyzed Carboxylation of Benzylic C–N Bonds with CO<sub>2</sub>. *Angew. Chem., Int. Ed.* **2016**, *55* (16), 5053–5057. (f) Liao, L. L.; Cao, G. M.; Ye, J. H.; Sun, G. Q.; Zhou, W. J.; Gui, Y. Y.; Yan, S. S.; Shen, G.; Yu, D. G. Visible-Light-Driven External-Reductant-Free Cross-Electrophile Couplings of Tetraalkyl Ammonium Salts. *J. Am. Chem. Soc.* **2018**, *140* (50), 17338–17342. (g) Jiang, W.; Li, N.; Zhou, L.; Zeng, Q. Copper-Catalyzed Stereospecific C–S Coupling Reaction of Enantioenriched Tertiary Benzylic Amines via *In Situ* Activation with Methyl Triflate. *ACS Catal.* **2018**, *8* (11), 9899–9906. (h) Scharfbier, J.; Gross, B. M.; Oestreich, M. Stereospecific and Chemoselective Copper-Catalyzed Deaminative Silylation of Benzylic Ammonium Triflates. *Angew. Chem., Int. Ed.* **2020**, *59* (4), 1577–1580.

(5) Katritzky, A. R.; Marson, C. M. Pyrylium Mediated Transformations of Primary Amino Groups into Other Functional Groups. *Angew. Chem., Int. Ed. Engl.* **1984**, *23* (6), 420–429.

(6) Basch, C. H.; Liao, J.; Xu, J.; Pian, J. J.; Watson, M. P. Harnessing Alkyl Amines as Electrophiles for Nickel-Catalyzed Cross Couplings via C–N Bond Activation. *J. Am. Chem. Soc.* **2017**, *139* (15), 5313–5316.

(7) (a) Li, Y.-N.; Xiao, F.; Guo, Y.; Zeng, Y.-F. Recent Developments in Deaminative Functionalization of Alkyl Amines. *Eur. J. Org. Chem.* **2021**, *2021* (8), 1215–1228. (b) Kong, D.; Moon, P. J.; Lundgren, R. J. Radical Coupling from Alkyl Amines. *Nat. Catal.* **2019**, *2* (6), 473–476.

(8) (a) Guan, W.; Liao, J.; Watson, M. P. Vinylation of Benzylic Amines via C–N Bond Functionalization of Benzylic Pyridinium Salts. *Synthesis* **2018**, *50* (16), 3231–3237. (b) Hoerner, M. E.; Baker, K. M.; Basch, C. H.; Bampo, E. M.; Watson, M. P. Deaminative Arylation of Amino Acid-derived Pyridinium Salts. *Org. Lett.* **2019**, *21* (18), 7356–7360. (c) Liao, J.; Basch, C. H.; Hoerner, M. E.; Talley, M. R.; Boscoe, B. P.; Tucker, J. W.; Garnsey, M. R.; Watson, M. P. Deaminative Reductive Cross-Electrophile Couplings of Alkylpyridinium Salts and Aryl Bromides. *Org. Lett.* **2019**, *21* (8), 2941–2946. (d) Liao, J.; Guan, W.; Boscoe, B. P.; Tucker, J. W.; Tomlin, J. W.; Garnsey, M. R.; Watson, M. P. Transforming Benzylic Amines into Diarylmethanes: Cross-Couplings of Benzylic Pyridinium Salts via C–N Bond Activation. *Org. Lett.* **2018**, *20* (10), 3030–3033. (e) Plunkett, S.; Basch, C. H.; Santana, S. O.; Watson, M. P. Harnessing Alkyl Pyridinium Salts as Electrophiles in Deaminative Alkyl-Alkyl Cross-Couplings. *J. Am. Chem. Soc.* **2019**, *141* (6), 2257–2262. (f) Wang, J.; Hoerner, M. E.; Watson, M. P.; Weix, D. J. Nickel-Catalyzed Synthesis of Dialkyl Ketones from the Coupling of N-Alkyl Pyridinium Salts with Activated Carboxylic Acids. *Angew. Chem., Int. Ed.* **2020**, *59* (32), 13484–13489. (g) Martin-Montero, R.; Yatham, V. R.; Yin, H.; Davies, J.; Martin, R. Ni-catalyzed Reductive Deaminative Arylation at sp<sup>3</sup> Carbon Centers. *Org. Lett.* **2019**, *21* (8), 2947–2951. (h) Yi, J.; Badir, S. O.; Kammer, L. M.; Ribagorda, M.; Molander, G. A. Deaminative Reductive Arylation Enabled by Nickel/Photoredox Dual Catalysis. *Org. Lett.* **2019**, *21* (9), 3346–3351. (i) Yue, H.; Zhu, C.; Shen, L.; Geng, Q.; Hock, K. J.; Yuan, T.;

Cavallo, L.; Rueping, M. Nickel-catalyzed C–N bond activation: activated primary amines as alkylating reagents in reductive cross-coupling. *Chem. Sci.* **2019**, *10* (16), 4430–4435. (j) Ni, S.; Li, C.-X.; Mao, Y.; Han, J.; Wang, Y.; Yan, H.; Pan, Y. Ni-catalyzed Deaminative Cross-electrophile Coupling of Katritzky Salts with Halides via C–N Bond Activation. *Sci. Adv.* **2019**, *5* (6), No. eaaw9516. (k) Sun, S. Z.; Romano, C.; Martin, R. Site-Selective Catalytic Deaminative Alkylation of Unactivated Olefins. *J. Am. Chem. Soc.* **2019**, *141* (41), 16197–16201.

(9) (a) Ociepa, M.; Turkowska, J.; Gryko, D. Redox-Activated Amines in C(sp<sup>3</sup>)–C(sp) and C(sp<sup>3</sup>)–C(sp<sup>2</sup>) Bond Formation Enabled by Metal-Free Photoredox Catalysis. *ACS Catal.* **2018**, *8* (12), 11362–11367. (b) Klauck, F. J. R.; James, M. J.; Glorius, F. Deaminative Strategy for the Visible-Light-Mediated Generation of Alkyl Radicals. *Angew. Chem., Int. Ed.* **2017**, *56* (40), 12336–12339. (c) Klauck, F. J. R.; Yoon, H.; James, M. J.; Lautens, M.; Glorius, F. Visible-Light-Mediated Deaminative Three-Component Dicarbofunctionalization of Styrenes with Benzylic Radicals. *ACS Catal.* **2019**, *9* (1), 236–241. (d) Jiang, X.; Zhang, M. M.; Xiong, W.; Lu, L. Q.; Xiao, W. J. Deaminative (Carbonylative) Alkyl-Heck-type Reactions Enabled by Photocatalytic C–N Bond Activation. *Angew. Chem., Int. Ed.* **2019**, *58* (8), 2402–2406. (e) Zhang, M.-M.; Liu, F. Visible-light-mediated allylation of alkyl radicals with allylic sulfones via a deaminative strategy. *Org. Chem. Front.* **2018**, *5* (23), 3443–3446. (f) Zhu, Z.-F.; Zhang, M.-M.; Liu, F. Radical alkylation of isocyanides with amino acid-/peptide-derived Katritzky salts via photoredox catalysis. *Org. Biomol. Chem.* **2019**, *17* (6), 1531–1534.

(10) (a) Wu, J.; He, L.; Noble, A.; Aggarwal, V. K. Photoinduced Deaminative Borylation of Alkylamines. *J. Am. Chem. Soc.* **2018**, *140* (34), 10700–10704. (b) Hu, J.; Wang, G.; Li, S.; Shi, Z. Selective C–N Borylation of Alkyl Amines Promoted by Lewis Base. *Angew. Chem., Int. Ed.* **2018**, *57* (46), 15227–15231. (c) Wu, J.; Grant, P. S.; Li, X.; Noble, A.; Aggarwal, V. K. Catalyst-Free Deaminative Functionalizations of Primary Amines by Photoinduced Single-Electron Transfer. *Angew. Chem., Int. Ed.* **2019**, *58* (17), 5697–5701. (d) James, M. J.; Strieth-Kalthoff, F.; Sandfort, F.; Klauck, F. J. R.; Wagener, F.; Glorius, F. Visible-Light-Mediated Charge Transfer Enables C–C Bond Formation with Traceless Acceptor Groups. *Chem. - Eur. J.* **2019**, *25* (35), 8240–8244.

(11) Hu, J.; Cheng, B.; Yang, X.; Loh, T. P. Transition-Metal-Free Deaminative Vinylation of Alkylamines. *Adv. Synth. Catal.* **2019**, *361* (21), 4902–4908.

(12) (a) Katritzky, A. R.; De Ville, G.; Patel, R. C. Carbon-alkylation of simple nitronate anions by N-substituted pyridiniums. *Tetrahedron* **1981**, *37* (Supplement 1), 25–30. (b) Marquet, J.; Moreno-Mañas, M.; Pacheco, P.; Prat, M.; Katritzky, A. R.; Brycki, B. C-alkylation of  $\beta$  diketones with benzylpyridinium salts. Evidence for chain radical mechanisms. *Tetrahedron* **1990**, *46* (15), 5333–5346. (c) Grimshaw, J.; Moore, S.; Trocha-Grimshaw, J. Electrochemical Reactions. Part 26. Radicals Derived by Reduction of N-Alkylpyridinium Salts and Homologous N,N'-Polymethylenebispyridinium Salts. Cleavage of the Carbon–Nitrogen Bond. *Acta Chem. Scand.* **1983**, *37b*, 485–489. (d) Itoh, M.; Nagakura, S. Preparation, ESR spectra and electronic absorption spectra of substituted pyridinyl radicals. *Tetrahedron Lett.* **1965**, *6* (8), 417–422.

(13) Katritzky, A. R.; Thind, S. S. The synthesis and reactions of sterically constrained pyrylium and pyridinium salts. *J. Chem. Soc., Perkin Trans. 1* **1980**, 1895–1900.

(14) Hansch, C.; Leo, A.; Taft, R. W. A survey of Hammett substituent constants and resonance and field parameters. *Chem. Rev.* **1991**, *91* (2), 165–195.

(15) Charton, M. Steric effects. III. Bimolecular nucleophilic substitution. *J. Am. J. Am. Chem. Soc.* **1975**, *97* (13), 3694–3697.

(16) When  $\sigma$  and  $\nu$  are each normalized to 1–2.3 ranges, the coefficient is still 40% larger for  $\sigma$  than  $\nu$ :  $\Delta G_{\text{red}}^0 = -21.52\sigma_p - 15.03\nu + 76.20$ .

(17) When  $\sigma$  and  $\nu$  are each normalized to 1–2.3 ranges, the coefficient is 14 times larger for  $\nu$  than  $\sigma$ :  $\Delta G_{\text{RD}}^\ddagger = -0.56\sigma_p - 8.05\nu + 29.05$ .

(18) Albright, T. A.; Burdett, J. K.; Whangbo, M.-H. Concepts of Bonding and Orbital Interaction. In *Orbital Interactions in Chemistry*; Albright, T. A., Burdett, J. K., Whangbo, M., Eds.; John Wiley & Sons, Inc.: 2013; pp 15–31.